Journal of Polymers and the Environment (2023) 31:886–899
https://doi.org/10.1007/s10924-022-02648-2

ORIGINAL PAPER

Sustainable Bio-Based Materials from Minimally Processed Red Seaweeds: Effect of Composition and Cell Wall Structure

Vera Cebrián-Lloret[1] · Antonio Martínez-Abad[1] · Amparo López-Rubio[1] · Marta Martínez-Sanz[2]

Accepted: 17 October 2022 / Published online: 5 November 2022

Abstract

This study reports on the use of whole seaweed biomass to obtain bio-based films for food packaging applications. Specifically, four different species of agarophytes (*Gelidium corneum, Gracilaria chilensis, Gracilaria tenuistipitata* and *Gracilariopsis longissima*) were minimally processed by melt blending and compression molding, and the effect of their composition and cell wall structure on the final performance of the films was investigated. The seaweed biomass was mainly composed of carbohydrates (35–50%), but significant amounts of proteins and ashes were also detected. Temperature-resolved SAXS experiments and microscopy analyses evidenced that a higher temperature of 130 ℃ is required to promote the release of agar from the tougher cell walls from *G. corneum* and *G. tenuistipitata*. The higher cellulose content of *G. corneum* (ca. 15%) resulted in films with higher mechanical resistance and water vapor barrier capacity, while the higher agar content of *G. chilensis* improved the elongation capacity of the films. The results from this work evidence the potential of red seaweed biomass to generate food packaging materials in a cost-effective and environmentally friendly way.

Keywords Biopolymers · Agar · Cellulose · Films · Macroalgae

Introduction

Plastics are one of the materials most widely used due to their low cost, good processability and wide range of barrier and mechanical properties. However, conventional petroleum-based plastics are not biodegradable and therefore accumulate in natural ecosystems for up to several thousand years after disposal, causing serious environmental problems [1–3]. As a more sustainable alternative, biodegradable polymers obtained from renewable natural resources, i.e. biopolymers, are being studied [4–6]. However, the properties of biopolymers are not yet comparable to those of benchmark synthetic polymers, especially in terms of mechanical and barrier properties. Even though for certain applications the properties of some biopolymers may be acceptable, their high production costs are one of the main factors precluding their commercialization. Moreover, the raw materials generally used for biopolymer production come from land-based crops, competing with their traditional use, the food sector. This is why, as an alternative, aquatic biomass sources such as marine plants or seaweeds are being explored [2, 4, 6–8].

Macroalgae are classified into three groups: Ochrophyta, Phaeophyceae (brown seaweeds), Chlorophyta (green seaweeds) and Rhodophyta (red seaweeds) [9–11] and their composition and cell wall structure is strongly dependent on the species. In particular, red seaweeds are rich in minerals and vitamins, as well as some bioactive compounds such as proteins, carotenoids, phenols or lipids [11, 12]. Furthermore, their high polysaccharide content makes them an abundant source of biopolymers. Of particular interest is agar, which is the main structural component of the cell walls in some red seaweed species [13]. It is composed of two main fractions: agarose, responsible for its gelling capacity, which consists of repeating units of alternating β-D -galactopyranosyl and 3,6-anhydro-α-L-galactopyranosyl groups; and agaropectin, which has a similar structure, but contains several substituent groups such as sulphates, methyl ethers and pyruvates [13, 14]. Due to its high gelling capacity, agar is widely used in the food and pharmaceutical industry [14, 15]. However, due to its excellent film-forming

✉ Marta Martínez-Sanz
marta.martinez@csic.es

[1] Food Safety and Preservation Department, IATA-CSIC, Avda. Agustín Escardino 7, 46980 Paterna, Valencia, Spain

[2] Instituto de Investigación en Ciencias de La Alimentación (CSIC-UAM), Nicolás Cabrera 9, 28049 Madrid, Spain

ability, in recent years its use in the production of food packaging materials has also been studied [16–19]. Although to a lesser extent, these seaweeds also have other polysaccharides of interest, such as cellulose, which also has a high potential for the development of bio-based food packaging [4] since, due to its semi-crystalline structure, it has excellent mechanical and barrier properties. However, due to the limited processability of cellulose, it is generally used as a filler to improve the properties of other biopolymers [4, 20].

The industrial processes for the extraction of agar and cellulose are time and energy consuming [13, 21]. To obtain biopolymeric materials for food packaging applications in a more energy efficient way, this study proposes to skip these extraction steps and produce packaging materials directly from seaweed biomass. This represents an innovative approach since, to the best of our knowledge, no previous works have reported on the production of pure seaweed based films before. To this end, four different species of agar-producing red seaweeds (*Gelidium corneum, Gracilaria chilensis, Gracilaria tenuistipitata* and *Gracilariopsis longissima*) have been minimally processed using the melt blending technique combined with compression molding, to produce films. The effect of the composition and cell wall structure of each seaweed species on the final performance of the films has also been investigated as a strategy for the optimization of these materials.

Materials and Methods

Raw Materials

The four red seaweeds [*Gelidium corneum* (formerly *Gelidium sesquipedale*), *Gracilaria chilensis, Gracilaria tinuistipitata* and *Gracilariopsis longissima* (formerly *Gracilaria verrucosa*)] were kindly donated by Hispanagar S.A. (Burgos, Spain). The dried seaweeds were ground to powder of particle size < 250 µm before further processing. Glycerol was purchased from Panreac Quimica, S.A. (Castellar Del Vallés, Barcelona, Spain).

Compositional Analysis and Antioxidant Properties

All the determinations were performed in triplicate, as follows.

Carbohydrate Analysis

Carbohydrate composition was determined by reductive hydrolysis following the protocol established by Stevenson & Furneaux with slight modifications [22, 23]. Briefly, 10 mg of dry sample was dissolved in a 5 mL aqueous rhamnose solution (0.5 mg/mL) for 40 min at 95 °C. Then, 0.5 mL of the solution was placed in Pyrex tubes and dried. A pre-hydrolysis step was conducted with 50 µL of 4-methylmorpholine-borane and 200 µL of 3 M trifluoroacetic acid were added to the tubes and placed in a heat block at 80 °C for 30 min. After cooling, 50 µL more 4-methylmorpholine-borane solution was added and the samples were dried. For the main hydrolysis, 200 µL of 2 M trifluoroacetic acid were added to the tubes and kept at 120 °C in the thermoblock for 1 h, followed by the addition of 100 µL of 4-methylmorpholine-borane and drying at 50 °C. After drying, the samples were resuspended in 1 mL H_2O, filtered through 0.45 µm syringe filters and transferred to chromatography vials. The monosaccharides were then analyzed using high-performance anion-exchange chromatography with pulsed amperometric detection (HPAEC-PAD) on an ICS-6000 (Dionex, ThermoFisher Scientific, Sunnyvale, CA, USA). Control samples of known concentrations of mixtures of glucose, galactose, rhamnose, 3,6-anhydro-L-galactose and 6-0-methyl-D-galactose were reduced to their corresponding alditols and used for calibration.

Protein Content

The protein content was estimated from the nitrogen content determined through the Dumas method, using an Elemental Analyser Rapid N Exceed (Paralab S.L., Spain), as described in [4]. The nitrogen content was multiplied by a factor of 6.25.

Ash Content

The mineral content of the dried seaweeds was determined by dry biomass calcination, according to the standard TAPPI T211 om-07 method, as described in [4].

Lipid Content

The lipid content of the dried seaweeds was determined gravimetrically according to AOAC method 991.36 [24] with some minor modifications, following the procedure described in [4].

Total Phenolic Content

The Folin-Ciocalteu technique was used to determine the total phenolic content of the dried seaweeds [25], following the protocol described in [4].

$ABTS^{\cdot+}$ Radical Cation Scavenging Activity

The dried seaweeds' $ABTS^{\cdot+}$ radical cation scavenging capacity was assessed according to [26], as detailed in [4].

Production of Seaweed-Based Films

Films based on seaweed biomass were prepared by melt compounding, followed by compression molding, using formulations based on mixtures of seaweed powder and water, with the addition of glycerol as a plasticizer (30% w/w with respect to the amount of seaweed powder in the mixture). For *G. corneum, G. chilensis* and *G. tenuistipitata* films, the seaweed powder: water ratio used was 1:4 (w/w), while a lower ratio of 1:5 (w/w) was used for the *G. longissima* film. These ratios were chosen based on preliminary tests to maintain a suitable balance between the generated films' mechanical integrity and proper processability. The different mixtures were melt-mixed in a Brabender Plastograph (Brabender GmbH, Duisburg, Germany) internal mixer at a temperature of 130 °C and 60 rpm for 4 min. These conditions were selected based on preliminary trials. Subsequently, 4 g of the obtained blends were spread evenly on Teflon films and placed in a compression mold (Carver 4122, USA) at a pressure of 16 tons and 130 °C for 4 min to form one film. The films were then stored in cabinets equilibrated at a relative humidity of 53% and 25 °C for at least 7 days.

Temperature-Resolved Small Angle X-ray Scattering (SAXS) Experiments

Small angle X-ray scattering (SAXS) experiments were carried out in the Non-Crystalline Diffraction beamline, BL-11, at ALBA synchrotron light source. The same formulations used to prepare the films were placed into sealed 1.5 mm quartz capillaries (Hilgenburg Gmbh, Germany) and analyzed. The energy of the incident photons was 12.4 keV or equivalently a wavelength, λ, of 1 Å. The SAXS diffraction patterns were collected by means of a Pilatus 1 M photon counting detector with an active area of 168.7×179.4 mm^2, an effective pixel size of 172×172 μm^2 and a dynamic range of 20 bits. The sample-to-detector distance was set to 7570 mm, resulting in a q range with a maximum value of q = 0.19 Å^{-1}. An exposure time of 1 s was selected based on preliminary trials. Samples were heated from 30 °C to 130 °C at a heating rate of 0.5 °C/min and frames of 1 s, followed by a period of 239 s in which the samples were protected from the beam by a local shutter. Each data frame corresponds to a temperature increase of 2 °C. The data reduction was treated by pyFAI python code (ESRF) [27], modified by ALBA beamline staff, to perform on-line azimuthal integrations from a previously calibrated file. The calibration files were created from a silver behenate standard. The radially averaged intensity profiles were then represented as a function of q using the IRENA macro suite [28] within the Igor software package (Wavemetrics, Lake Oswego, Oregon).

Optical Microscopy

The seaweed aqueous solutions were analyzed by optical microscopy. Images were captured using a Nikon Eclipse 90i microscope with a 5-megapixel Nikon Digital Sight DS-5Mc cooled digital color microphotography camera (Nikon Corporation, Japan). Images of the materials were also captured using a fluorescent filter UV-2A (Excitation 330–380 nm, Dichroic Mirror 400, and LongPass 420 nm for emission). Nis-Elements Br 3.2 Software was used to analyze, and process acquired pictures (Nikon corporation, Japan).

X-ray Diffraction (XRD)

XRD measurements were performed using a Bruker diffractometer model D5005. The instrument was equipped with a secondary monochromator and a Cu tube. The configuration of the equipment was θ–2θ, and the samples were examined over the angular range of 3°–60° with a step size of 0.02° and a count time of 200 s per step. Peak fitting was carried out using the Igor software package (Wavemetrics, Lake Oswego, Oregon), using the same protocol described in a previous work [13]. The obtained values from the fitting coefficients are those that minimize the value of Chi-squared, which is defined as:

$$\chi^2 = \sum \left(\frac{y - y_i}{\sigma_i} \right)^2, \quad (1)$$

where y is a fitted value for a given point, y_i is the measured data value for the point and σ_i is an estimate of the standard deviation for y_i. The curve fitting operation is carried out iteratively and for each iteration, the fitting coefficients are refined to minimize χ^2. The crystallinity index was determined from the obtained fitting results by applying the following equation:

$$X_C(\%) = \frac{\sum A_{Crystal}}{A_{Total}} \times 100, \quad (2)$$

where A_{Total} is the sum of the areas under all the diffraction peaks and $\Sigma A_{Crystal}$ is the sum of the areas corresponding to the crystalline peaks.

Thermogravimetric Analyses (TGA)

Thermogravimetric curves (TG) were recorded with a TA 550 (Waters- TA Instruments, New Castle, EEUU). Under an oxygen environment, the samples (5 mg) were heated at a rate of 10 °C/min from 30 to 800 °C. Derivative TG

curves (DTG) express the weight loss rate as a function of temperature.

Scanning Electron Microscopy (SEM)

SEM experiments were carried out using a Hitachi S-4800 microscope with an accelerating voltage of 10 kV and a working distance of 8–16 mm. Before their morphology was evaluated, small sections of the seaweed films were sputtered with a gold–palladium combination under vacuum for 2 min.

Contact Angle Measurements

Contact angle measurements were carried out in a DSA25 equipment (Krüss, Hamburg, Germany) equipped with image analysis AD4021 software at ambient conditions. Using a precision syringe, a water droplet (3 µL) was placed on the film's surface. Contact angle values were obtained by analyzing the shape of the water drop after it had been placed over the film for 10 s. Results were obtained from an average of at least 5 measurements.

Water Vapor Permeability (WVP)

Direct permeability to water was determined from the slope of the weight gain versus time curves at 24 °C, following the same method described in [4]. The tests were done at least in triplicate.

Water Sorption

The water sorption capacity of the films was evaluated by registering the weight gain, using an analytical balance, when placing the samples in a cabinet equilibrated at 25 °C and 100% RH. Square samples with a total surface area of 6.25 cm^2 were cut from the films and their initial weight was registered. The assays were carried out at least in triplicate.

Mechanical Properties

Tensile tests were performed at ambient conditions on a universal test Machine (Instron, USA), according to the method described in [4]. The stress–strain curves were used to determine the elastic modulus (E), tensile strength (TS), and elongation at break (ε_B) of the films. At least, three specimens of each film were tested.

Statistics

The average ± standard deviation has been used to represent all the data. Different letters show significant differences in both graphs and tables. ($p \leq 0.05$). Analysis of variance (ANOVA) followed by a Tukey-test were used.

Results and Discussion

Compositional Characterization of the Dried Seaweeds

To understand the impact of the seaweed choice on the processability and functional properties of the films obtained by minimal processing, the composition and the antioxidant capacity of the different agarophytes were investigated.

As observed in Table 1, all seaweeds were mainly composed of structural carbohydrates (i.e., agar and cellulose), ashes and proteins. When comparing the four seaweeds, it could be observed that *G. corneum* presented the highest protein content (ca. 19%) and the lowest carbohydrate (ca. 35%) and lipid content (ca. 5%). It should be highlighted that despite its lowest carbohydrate content, the amount of cellulose was the highest in this seaweed (ca. 14%). Interestingly, although the agar content (ca. 21%) was the lowest compared to the other seaweed species, almost 97% of it consisted of agarose, i.e., the fraction that provides gelling capacity. Although a detailed characterization of the composition of *Gelidium corneum* is not available in the existing literature,

Table 1 Composition and antioxidant capacity of the dried seaweeds

	Protein (%)	Mineral (%)	Lipid (%)	Carbohydrate (%)		Polyphenol (mg GAE/g sample)	Antioxidant capacity ABTS (mg TE/g sample)
				Agar*	Cellulose		
G. corneum	19.4 ± 0.5^{d}	9.2 ± 0.05^{a}	4.7 ± 0.6^{a}	21 ± 0.5 [97]^{a}	14.2 ± 1.2^{c}	15 ± 0.9^{d}	3.8 ± 0.5^{a}
G. chilensis	18.6 ± 0.06^{c}	9.6 ± 0.1^{a}	9.1 ± 0.9^{c}	43.7 ± 6 [77]^{d}	5.9 ± 0.2^{a}	11.1 ± 0.3^{c}	12.6 ± 0.6^{c}
G. tenuistipitata	15.5 ± 0.09^{b}	23.3 ± 0.4^{b}	4.8 ± 1^{a}	30.7 ± 4 [92]^{b}	6.1 ± 0.02^{a}	6.3 ± 0.3^{b}	7.6 ± 0.6^{b}
G. longissima	8 ± 0.04^{a}	28 ± 1.3^{c}	6.9 ± 0.6^{b}	29.7 ± 3.7 [74]^{c}	9.5 ± 0.4^{b}	1 ± 0.2^{a}	9.4 ± 0.05^{d}

Values within the same column with different letters are significantly different ($p \leq 0.05$)

*The value in brackets corresponds to the percentage purity in agarose of each agar fraction as determined by HPAEC-PAD after reductive hydrolysis

other *Gelidium* species have been reported to have a similar composition [29, 30].

Despite belonging to the *Gracilaria* genera, the other three seaweed species showed significant differences in their composition. *Gracilariopsis longissima* presented the highest cellulose content (ca. 10%) and the lowest agar content (ca. 30%), with almost 26% of it constituted by agaropectin. *G. chilensis* and *G. tenuistipitata* exhibited very similar cellulose (ca. 6%) and protein (ca. 19 and 16%, respectively) contents, but significantly differed in their agar concentration. In fact, *G. chilensis* was the species with the highest agar content (ca. 44%), although its agaropectin fraction was also quite high (ca. 23%). In contrast, *G. tenuistipitata,* showed a lower agar content (ca. 31%), but consisted of almost 93% agarose. Also noticeable was the high mineral content of all species, in agreement with previous values reported for red seaweeds, being significantly higher in *G. tenuistipitata* and *G. longissima* (ca. 23 and 28%, respectively). The lipid content, constituting up to ca. 9% of *G. chilensis* composition, was higher than the values previously reported for several *Gracilaria* species [29]. However, it should be noted that a great variability in the composition of the different species of the *Gracilaria* genera has been reported in the literature [29, 31–33]. This is also related to the fact that the chemical composition of seaweeds does not only vary according to the species, but also due to other aspects such as habitat, seasonality, maturity and environmental conditions [12, 34, 35]. Phenolic compounds, which are known to present antioxidant properties, have also been reported to be present in red seaweeds (up to ca. 20 mg GAE/g sample for extracts of various species of the *Gracilaria* genera [36–38], or up to 14.1 mg GA/g sample for species of the *Gelidium* genera [39], although it is difficult to find consistent values on their antioxidant capacity. Regarding polyphenol content, *G. corneum* showed the highest one (ca. 15 mg GAE/g sample), followed *by G. chilensis* and *G. tenuistipitata* with ca. 11.1 and 6 mg GAE/g sample respectively, while *G. longissima* presented the lowest content (ca. 1 mg GAE/g sample). However, although the antioxidant capacity of seaweeds is usually linked to the presence of polyphenols, our results evidence that the antioxidant capacity may be also linked to the presence of other bioactive compounds such as sulphated polysaccharides (e.g., agaropectin) and lipids. In particular, *G. chilensis*, presenting the highest agar and lipid content from all the species, showed the highest antioxidant capacity (12.6 mg TE/g sample), while the lowest antioxidant capacity was obtained for *G. corneum*, the seaweed with the lowest agar and lipid content.

Structural Effects of Processing Temperature

To determine the optimal processing conditions for the production of the films, preliminary tests were carried out in which aqueous dispersions of the four seaweeds were subjected to temperatures from 30 °C up to 130 °C and their nanostructure was characterized by means of SAXS. The scattering patterns obtained at selected temperatures were graphically represented in Kratky plots to enhance the visualization of structural features.

As observed in Fig. 1, the temperature had a clear effect on all seaweeds, with the scattering intensity generally increasing as the temperature was raised. This may be explained by the diffusion of agar from the interior of the cell walls towards the liquid medium when increasing the temperature, hence increasing the scattering length density of the whole suspensions. In fact, a shoulder feature centered at $q = 0.015$ Å^{-1} was detected in the *G. corneum* suspension heated at 130 °C. Similar features have been previously detected in the SAXS patterns from agars [40] and although their origin is still uncertain, they have been hypothesized to be originated by a form factor effect associated with the length of the agarose double helices. Interestingly, in *G. chilensis* and *G. longissima*, the scattering intensity decreased when raising the temperature from 110 to 130 °C. This may be originated by the disruption of the double helical structure in the agarose fraction when reaching high temperatures. The semi-crystalline structure of agarose double helices is thought to provide higher scattering contrast with the solvent than the amorphous agaropectin domains. It is reasonable to hypothesize that the smaller fraction of semi-crystalline agarose in these two seaweed species is disrupted more quickly when increasing the temperature, hence producing a decrease in the scattering intensity.

In addition, several small scattering peaks were detected within the high q region in all samples. In *G. corneum*, i.e., the seaweed with the highest cellulose content, a weak peak centered at ca. 0.14 Å^{-1} (corresponding to a real distance of ca. 4.5 nm) was observed in the suspension at 30 °C and shifted towards lower q values when heating above 90 °C. The shape and position of this peak is very similar to that previously reported for other cellulose-rich sources, such as cotton, in the dry state [8]. This interference peak has been related to the center-to-center distance between the cellulose microfibrils, which in the dry state are closely packed together. The fact that this peak could be observed in the aqueous suspensions indicates a high degree of packing even in the hydrated state, in contrast to other cellulosic sources were water can easily penetrate the space between the microfibrils and increase their interspacing distance [8, 41]. This weak peak was also observed in *G. chilensis* and *G. tenuistipitata*, although its position was slightly different depending on the species. In the case of *G. tenuistipitata*, the peak appeared at 0.08 Å^{-1} (corresponding to a real distance of ca. 8.1 nm) for the suspension at 30 °C, while it shifted towards higher q when raising the temperature (being centered at 0.09 Å^{-1} when the sample reached 130 °C).

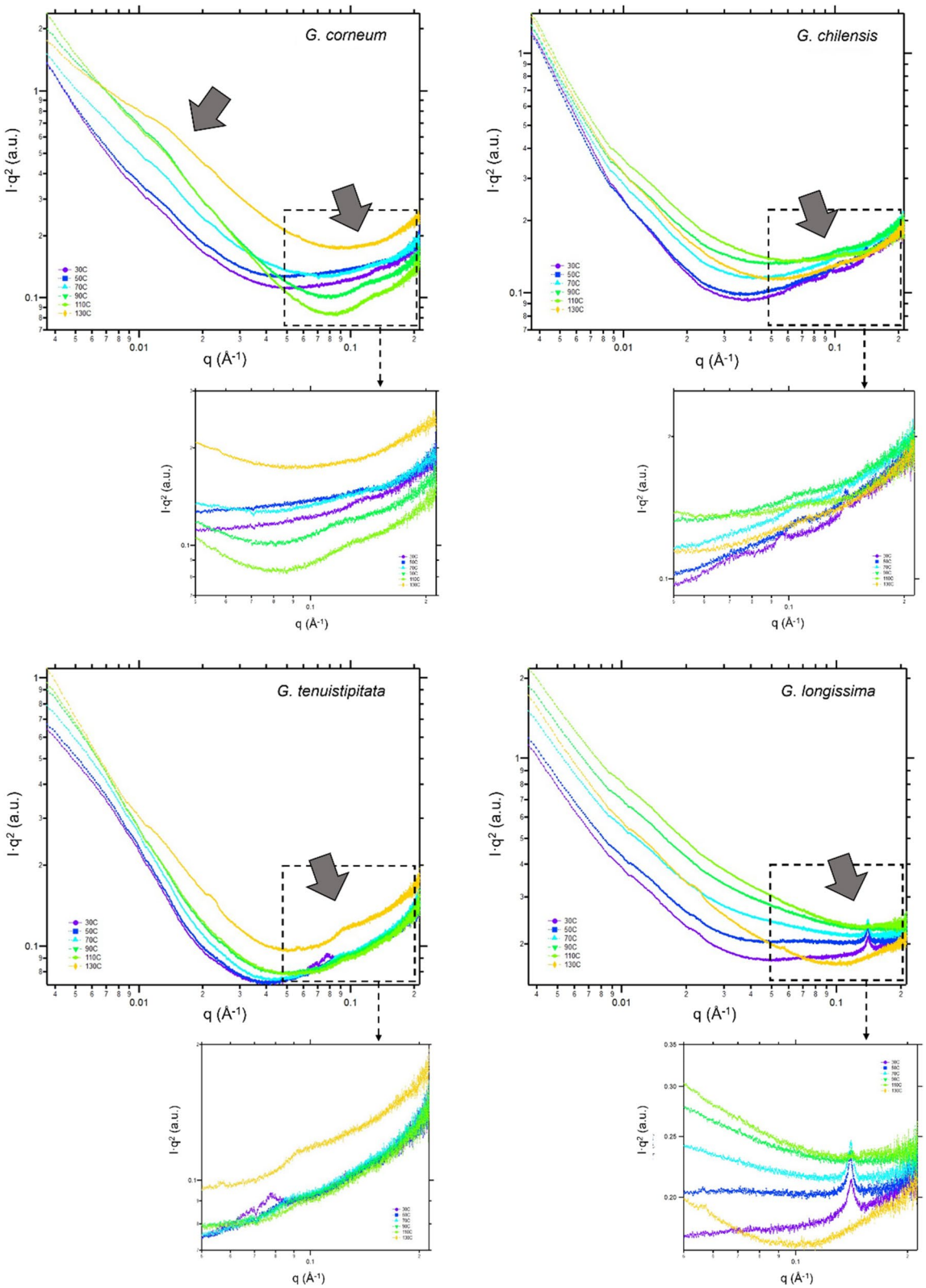

Fig. 1 SAXS Kratky plots of seaweed aqueous dispersions processed at different temperatures from 30 to 130 °C. The arrows point towards structural peaks, which are more clearly visualized in the insets

In *G. chilensis*, two peaks were detected at temperatures up to 90 °C; the first one was located at 0.10 $Å^{-1}$ (real distance of ca. 6.5 nm) at 30 °C and shifted towards higher q when increasing the temperature, whereas the second peak was located at 0.14 $Å^{-1}$ (real distance of ca. 4.5 nm). In *G. longissima*, a sharper and more intense peak, located at 0.14 $Å^{-1}$, was detected for temperatures up to 110 °C. The sharper appearance of this peak in *G. longissima* may be explained by the relatively high cellulose content of this seaweed (as compared to the other species) and its low agarose content, thus originating higher contrast between the crystalline cellulose and the amorphous agaropectin.

It should be noted that while an interfibrillar distance of 4.5 nm corresponded to the species with the highest cellulose content (i.e., *G. corneum* and *G. longissima*), which is very similar to the values previously reported for dry cotton and bacterial cellulose [8, 41], greater distances were detected for the other two species, which was presumably due to the presence of other polysaccharides interacting with cellulose and increasing the distance between microfibrils. Furthermore, increasing the temperature in the suspensions may have promoted the penetration of water within the interfibrillar space and/or affected the conformation of non-cellulosic polysaccharides, hence modifying the distance between the microfibrils.

The effect of temperature on the cell structure of the different seaweeds was also studied through optical microscopy. The seaweed aqueous suspensions were examined after reaching temperatures of 110 and 130 °C (above the melting temperature of agar). Figure 2 shows representative images taken with bright light and ultraviolet filters.

The images taken with bright light clearly show changes in the morphology of the seaweeds when the temperature increased. In particular, the rough edges of the seaweed cells became less defined and the cell size increased. This swelling effect was less noticeable in *G. corneum* while it was much more evident in *G. chilensis* and *G. longissima*. The increase in the temperature in the presence of moisture is expected to promote the melting of the agar contained within the seaweed cell walls, which may be able to diffuse towards the liquid medium. It seems that the high cellulose content in *G. corneum*, yielding tough cell walls, together with the high agarose/agaropectin ratio, did not favour the diffusion of agar. On the contrary, the lower agarose/agaropectin ratio in *G. chilensis* and *G. longissima* seemed to promote agar diffusion. This is further supported by the observation of the samples under the UV filter. While the images of the unprocessed native seaweeds were mostly dominated by the appearance of bright blue fluorescent regions, the images of the processed seaweeds showed very faint to no light blue fluorescence. According to compositional analyses, it may be hypothesised that the blue fluorescent areas correspond to agar-rich regions, which disappear almost completely after processing (especially at 130 °C) indicating the release of agar from the cell walls. In all cases it seems that increasing the temperature from 110 to 130 ºC produced a greater release of the agar, which would be, in principle, more optimum for the production of the seaweed-based films.

It should be noted that temperatures higher than 130 °C were not suitable to process these seaweeds since some degradative processes (Maillard reactions, glycerol thermal degradation, polyphenol degradation, etc.) led to a substantial detriment in the mechanical properties of the obtained films.

Characterization of the Seaweed-Based Films

Once the optimum processing temperature of the seaweeds was determined, the films were produced by melt mixing, followed by compression molding. Figure 3 shows the visual appearance of the films. As expected, due to the variety of compounds present in the seaweed biomass, all of them were opaque with a brownish coloration, similar to that previously observed in films produced from less purified agars extracted from *G. corneum* [17].

The films' surface morphology was analyzed by SEM and representative images are shown in Fig. 3. Due to the addition of glycerol, small particles homogeneously distributed over the whole surface of the films were visible in all samples. However, a noticeable morphological difference was observed between the films made from *G. corneum* and the films based on *Gracilaria* species. While the *G. corneum* film exhibited a more homogeneous surface, where only the glycerol particles were visible, the films based on *Gracilaria* species showed significantly rougher surfaces, fact which could be related to the greater swelling of the cell walls from these species, generating larger particles.

TGA analyses were carried out to determine the thermal stability of the films. The derivative of the weight loss with temperature was plotted and the results are shown in Fig. 4.

The films showed a multistep degradation mechanism, which was mostly dominated by a strong peak around 270–280 °C, attributed to agar degradation [42, 43]. All the samples exhibited a small degradation step centered around 150 °C, which may be attributed to moisture loss and glycerol degradation [19, 42, 44]. The degradation steps centered around 230 °C, which may be attributed to the presence of proteins [4], and at 330 °C attributed to cellulose [4, 45], although present in all samples, were more evident in the film made from *G. corneum.* This indicates that a multiphase structure was attained in the films from *G. corneum*, which can be linked to the fact that this seaweed species is structurally less affected by the melt mixing temperature than the *Gracilaria* seaweeds, as evidenced by optical microscopy (cf. Figures 2).

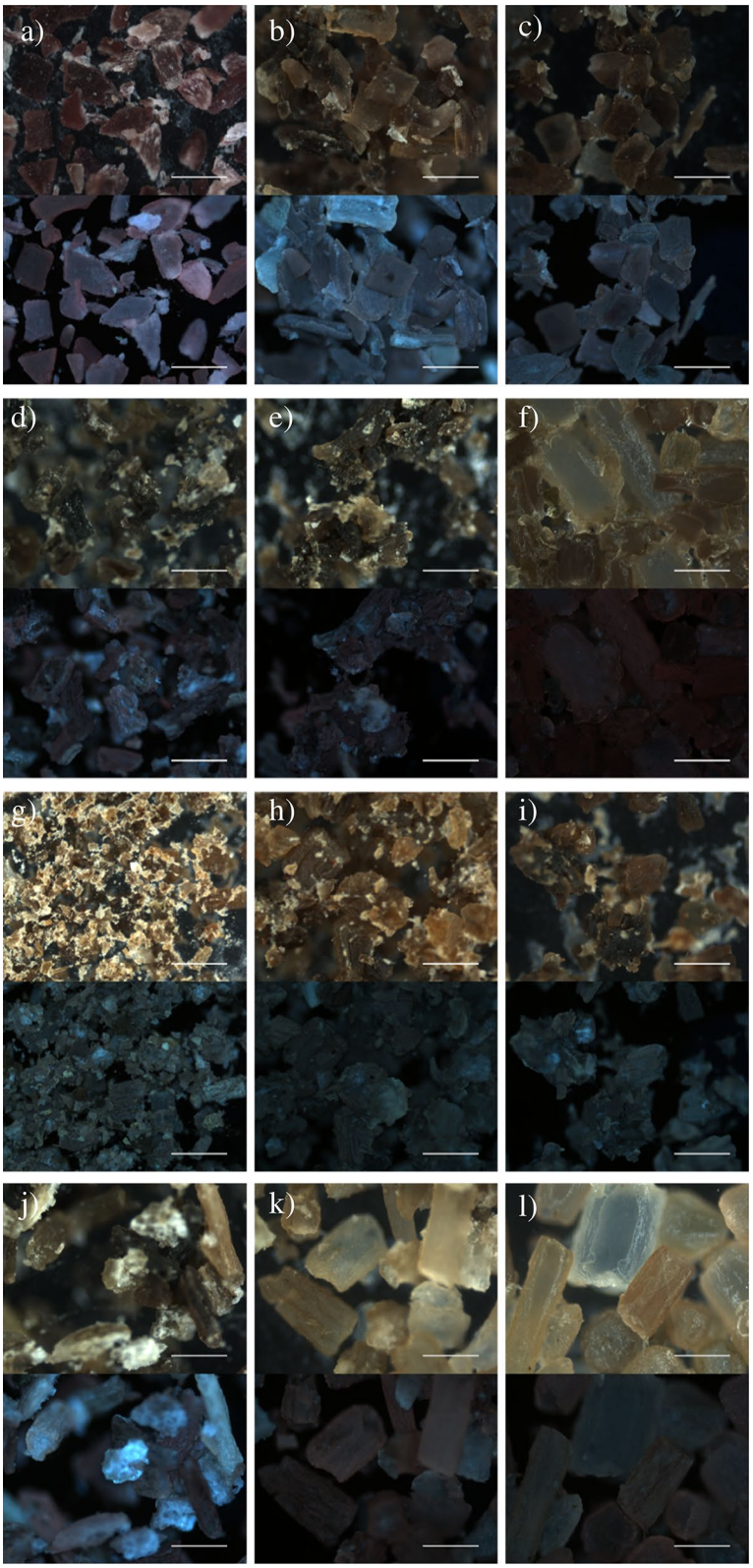

Fig. 2 Optical microscopy images of seaweed aqueous suspensions in their native state (**a**, **d**, **g**, **j**) and after being processed at 110 ℃ (**b**, **e**, **h**, **k**) and 130 ℃ (**c**, **f**, **i**, **l**) for *G. corneum*, (**a**, **b**, **c**) *G. chilensis*, (**d**, **e**, **f**) *G. tenuistipitata,* (**g**, **h**, **i**) and *G. longissima* (**j**, **k**, **l**). Scale bars correspond to 500 µm. Top images were taken with bright light while bottom images were taken using a fluorescent filter UV-2A

XRD analyses were carried out to investigate the crystalline structure of the produced films and the obtained patterns are shown in Fig. 5.

As observed, all the films presented a broad diffraction band within the range of 12-25º with a maximum at 19º, similar to the patterns reported for agar-based films [13, 46].

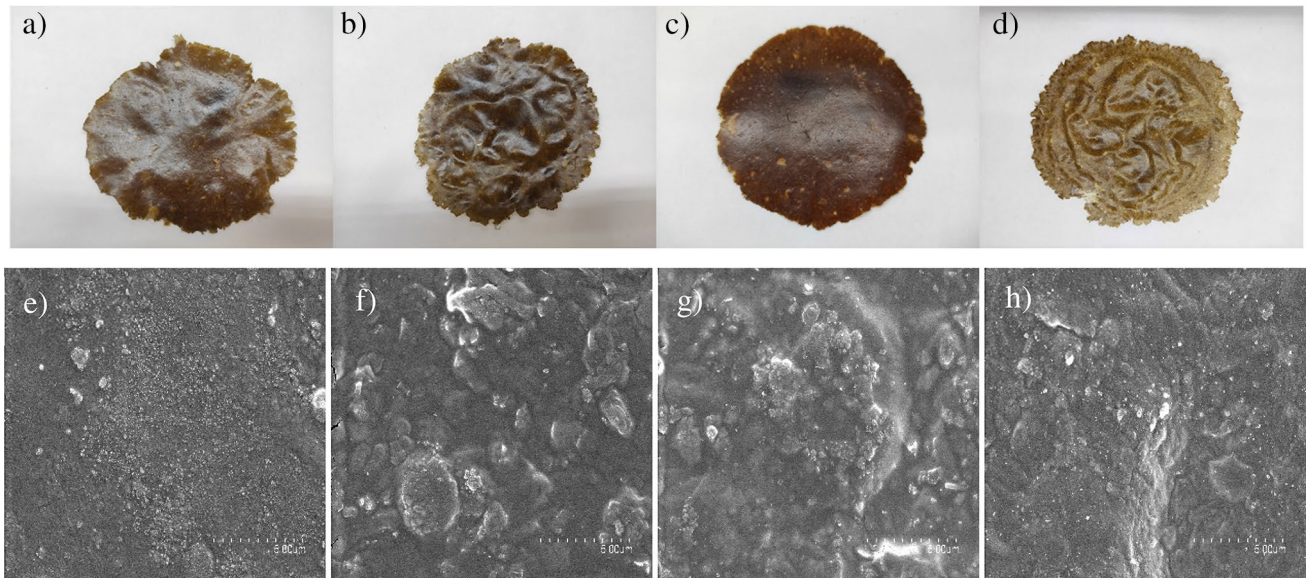

Fig. 3 Visual appearance (**a**–**d**) and SEM images (**e**–**h**) of the seaweed-based films: *G. corneum* (**a**, **e**), *G. chilensis* (**b**, **f**), *G. tenuistipitata* (**c**, **g**), *G. longissima* (**d**, **h**)

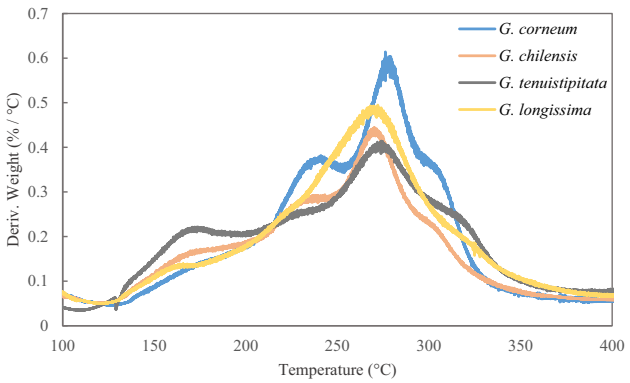

Fig. 4 TGA derivative curves of the seaweed-based films

Furthermore, in the *G. corneum* films and also, more subtly, in the *G. longissima* films, a peak centered at 22.5º, related to the crystalline structure of cellulose I [47] was also noticeable. This is consistent with the higher cellulose content present in these seaweed species. Several sharp and intense peaks could also be observed in the films from *G. tenuistipitata* and, to a lesser extent, from *G. chilensis*. These peaks may be attributed to the presence of mineral compounds, such as silica (SiO_2) and weddellite ($CaC_2O_4{\cdot}2H_2O$), which have been previously detected in the XRD spectra of some red seaweeds [13].

The crystallinity of the films was estimated by fitting the areas under the diffraction patterns and, as deduced from the values shown in Table 2, *G. tenuistipitata* and *G. corneum* films presented a more crystalline structure. However, it should be considered that, for the calculation of the overall crystallinity, other components such as cellulose and minerals are also contemplated and, therefore, the values are not indicative of the degree of crystallinity of the agar. Looking at the values calculated only considering the crystalline peak corresponding to agar, it is evident that those seaweeds with the greatest agarose/agaropectin ratio (i.e., *G. corneum* and *G. tenuistipitata*) presented a more crystalline agar structure. On the other hand, despite being the species with the greatest overall polysaccharide content, the film from *G. chilensis* presented the most amorphous behavior, which may be ascribed to the greater proportion of agaropectin in this seaweed.

To evaluate the potential of the films as food packaging materials, their performance properties were also characterized. The mechanical properties were assessed by means of tensile testing and the most representative parameters obtained from the stress–strain curves are summarized in Table 2.

As expected, due to its higher cellulose content, *G. corneum* resulted in stiffer (E ≈1213 MPa) and more resistant (σ ≈ 14.1 MPa) films with a lower elongation at break (εb ≈ 1.8%). In contrast, the higher agar and lower cellulose content of *G. chilensis* significantly decreased the elastic modulus (E ≈ 581 MPa) and tensile strength of the film (σ ≈ 9.6 MPa) but improved its ductility (εb ≈ 4.9%). *G. tenuistipitata* and *G. longissimaa*, showed non-significant differences between them in terms of stiffness and elongation at break. However, the higher cellulose content of *G. longissima* improved the tensile strength of the films. When comparing the results obtained for seaweed-based films with those reported for some reference biopolymers

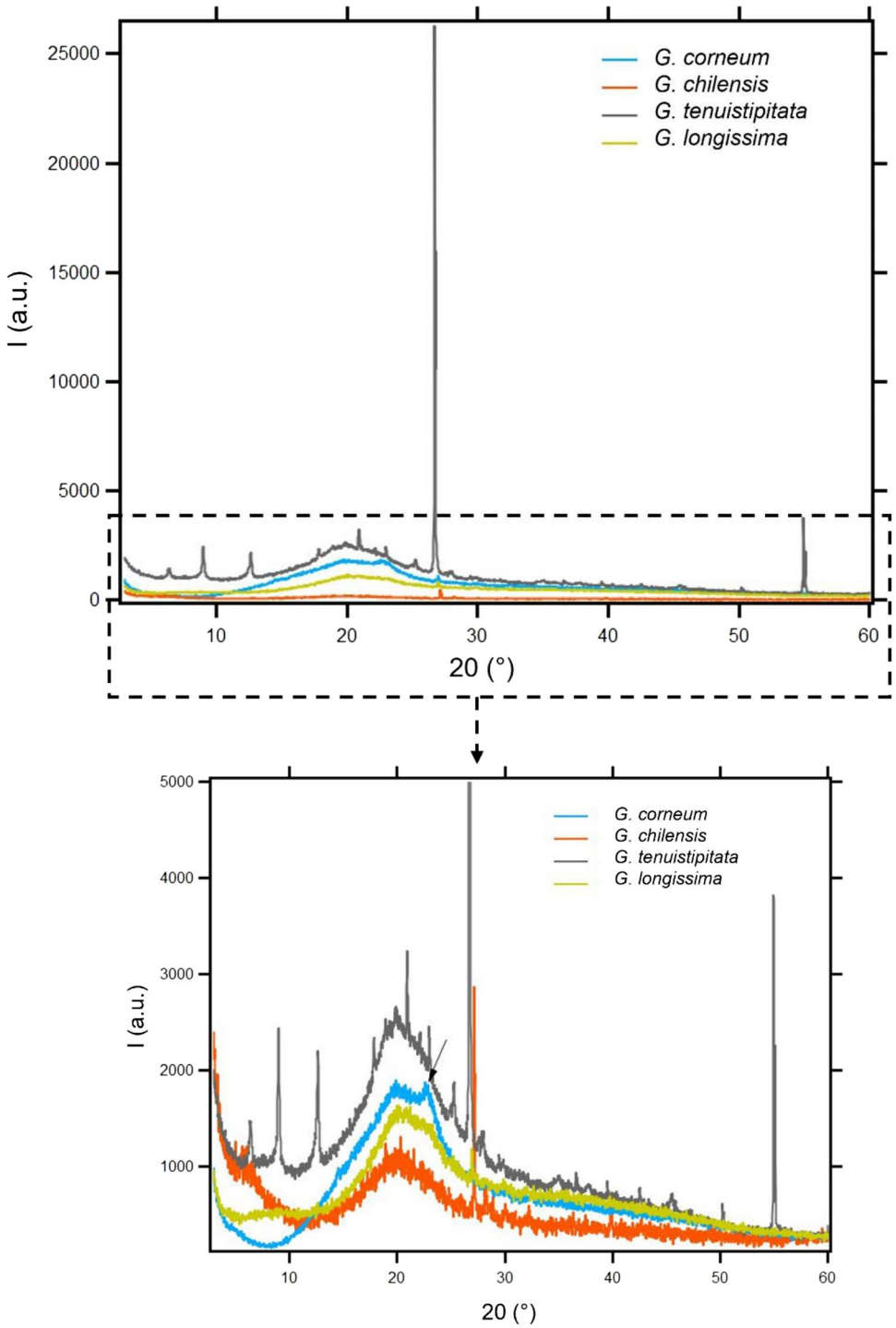

Fig. 5 XRD patterns of the seaweed-based films

such as PLA (E = 3290 MPa, σ = 49.6 MPa, εb = 2.4%) [48, 49] or thermoplastic starch (E = 29.8 MPa, σ = 3.1 MPa, εb = 62.6%) [50, 51] it can be noted that the minimal processing method of seaweeds results in biofilms with an intermediate behavior between that from PLA and thermoplastic starch in terms of mechanical properties. Furthermore, the mechanical properties are also comparable to those reported for agar films processed by casting (E = 29–1600 MPa, σ = 6–38 MPa, ε_B = 15–26%) [17, 52].

The water vapor permeability (WVP) of the films was also characterized and the results, gathered in Table 2, suggest that the seaweeds with the highest cellulose content (i.e., *G. longissima* and *G. corneum*) produced films with a better barrier capacity. As seen in previous studies, this

Table 2 Crystallinity, mechanical and water barrier properties of the seaweed-based films

	Xc (%)*	E (MPa)	σ (MPa)	ε_b (%)	$P_{H2O} \cdot 10^{-13}$ (kg·m/s·m^2·Pa)	Water sorption (%)
G. corneum	50 [44]	1213 ± 95^{c}	14.1 ± 1.5^{c}	1.8 ± 0.17^{a}	1.6 ± 0.08^{ab}	130 ± 4^{a}
G. chilensis	27 [25]	581 ± 42^{a}	9.6 ± 0.4^{a}	4.9 ± 0.26^{c}	1.9 ± 0.17^{b}	–
G. tenuistipitata	62 [46]	748 ± 70^{b}	9.9 ± 1^{a}	2.9 ± 0.06^{b}	1.8 ± 0.05^{b}	–
G. longissima	40 [31]	749 ± 10^{b}	11.6 ± 0.7^{b}	2.5 ± 0.2^{b}	1.4 ± 0.02^{a}	152 ± 1^{b}

X_C Crystallinity index; E Young's modulus; σ tensile strength; ε_b elongation at break; P_{H2O} water permeability

Values within the same column with different letters are significantly different ($p \leq 0.05$)

*The crystallinity values estimated by considering only the agar characteristic peaks are shown between brackets

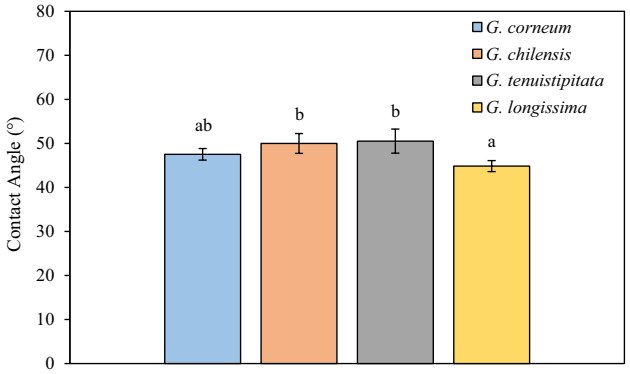

Fig. 6 Water contact angle measurements of the seaweed-based films

may be due, amongst other factors, to the reduced amount of free hydroxyl groups due to the interactions established between cellulose and agar [4, 17]. As previously reported, both agar and cellulose have a high barrier capacity [4, 17, 45, 53]. Even so, it is surprising that these films, made from seaweed biomass without any purification process, presented WVP values comparable to those reported for pure cellulose films extracted from aquatic biomass sources such as *Arundo donax* (terrestrial angiosperm) [54] or *Posidonia oceanica* (marine angiosperm) [55], as well as films made from unpurified agar-based extracts [17]. Interestingly, the cellulose content seemed to be the prevailing factor controlling the permeability, rather than the overall crystallinity of the films.

To evaluate the sensitivity of the films to moisture, their water sorption capacity was also measured. While the films from *G. corneum* and *G. longissima* maintained their structure throughout the experiment, the films made from *G. chilensis* and *G. tenuistipitata* disintegrated over time. Therefore, in line with the water vapor barrier capacity, this indicates that seaweeds with a higher cellulose content result in films with a higher structural stability to moisture.

Interestingly, the films made from *G. longissima* and *G. corneum*, exhibited a slightly more hydrophilic surface than the films made from *G. tenuistipitata* and *G. chilensis*, as evidenced by the contact angle measurements (cf. Figure 6). This may be due, amongst other factors, to the higher agar and protein content of the two latter species, since, as previously reported, protein/polysaccharide interactions can have a hydrophobising effect on the surface of the films [56]. In general, seaweed-based films showed a similar behavior to that reported for films based on some polysaccharides such as agar (50°) [53] or cellulose nano whiskers (44°) [57].

Conclusions

Four different agarophyte species were minimally processed by melt blending combined with compression molding and the effect of the composition and cell wall structure of the different species on film performance were investigated. The seaweed biomass was mainly composed of carbohydrates (35–50%), but significant amounts of protein and ashes were also detected. *G. corneum* showed the highest cellulose content (ca. 15%) and the lowest agar content (ca. 21%), although it contained the highest agarose ratio (97%). *G. tenuistipitata* also showed a relatively low agar content (ca. 31%) of which almost 93% was agarose. In contrast, the agar fraction in *G. chilensis* and *G. longissima* contained a significant proportion of agaropectin, with the latter one having a relatively high amount of cellulose (ca. 10%). The greater cellulose content in *G. corneum* limited the diffusion of agar when seaweed aqueous suspensions were processed at high temperatures, while the more amorphous character of the agar in *G. chilensis* and *G. longissima* promoted its diffusion towards the liquid medium. In any case, increasing the temperature to 130 °C seemed to promote a greater release of agar.

The cellulose content seemed to be the main factor controlling the mechanical and water barrier performance of the films. The higher cellulose content of *G. corneum* resulted in stronger films with high water vapor barrier capacity, while the higher agar content of *G. chilensis* improved its elongation capacity. The films made from *G. longissima* also showed interesting properties due to the relatively high cellulose content, thus offering an interesting alternative to

produce biopolymeric films. The results from this work evidence the potential of red seaweed biomass to generate food packaging materials in a cost-effective and environmentally friendly way.

Author Contributions All authors contributed to the study conception and design. Material preparation, data collection and analysis were performed by all authors. The first draft of the manuscript was written by VC-L and all authors commented on previous versions of the manuscript. All authors read and approved the final manuscript.

Funding Open Access funding provided thanks to the CRUE-CSIC agreement with Springer Nature. This work was financially supported by Hispanagar. Synchrotron experiments were performed at NCD beamline at ALBA Synchrotron with the collaboration of ALBA staff (2020024090 project).

Data Availability The datasets generated during and/or analysed during the current study are available from the corresponding author on reasonable request.

Declarations

Competing Interests The authors have no relevant financial or non-financial interests to disclose.

References

1. Doh H, Dunno KD, Whiteside WS (2020) Preparation of novel seaweed nanocomposite film from brown seaweeds *Laminaria japonica* and *Sargassum natans*. Food Hydrocoll 105:105744. https://doi.org/10.1016/J.FOODHYD.2020.105744
2. Abdul Khalil HPS, Saurabh CK, Tye YY et al (2017) Seaweed based sustainable films and composites for food and pharmaceutical applications: a review. Renew Sustain Energy Rev 77:353–362
3. Otari SV, Jadhav JP (2021) Seaweed-based biodegradable biopolymers, composite, and blends with applications. Bioremediation using weeds. Springer, Berlin, pp 121–149
4. Cebrián-Lloret V, Metz M, Martínez-Abad A et al (2022) Valorization of alginate-extracted seaweed biomass for the development of cellulose-based packaging films. Algal Res 61:102576. https://doi.org/10.1016/J.ALGAL.2021.102576
5. Fathiraja P, Gopalrajan S, Karunanithi M et al (2021) Response surface methodology model to optimize concentration of agar, alginate and carrageenan for the improved properties of biopolymer film. Polym Bull. https://doi.org/10.1007/s00289-021-03797-5
6. Martínez-Sanz M, Cebrián-Lloret V, Mazarro-Ruiz J, López-Rubio A (2020) Improved performance of less purified cellulosic films obtained from agar waste biomass. Carbohydr Polym. https://doi.org/10.1016/j.carbpol.2020.115887
7. Kartik A, Akhil D, Lakshmi D et al (2021) A critical review on production of biopolymers from algae biomass and their applications. Bioresour Technol 329:124868. https://doi.org/10.1016/J.BIORTECH.2021.124868
8. Martínez-Sanz M, Pettolino F, Flanagan B et al (2017) Structure of cellulose microfibrils in mature cotton fibres. Carbohydr Polym 175:450–463. https://doi.org/10.1016/J.CARBPOL.2017.07.090
9. Leandro A, Pereira L, Gonçalves AMM (2020) Diverse applications of marine macroalgae. Mar Drugs 18:17
10. Øverland M, Mydland LT, Skrede A (2018) Marine macroalgae as sources of protein and bioactive compounds in feed for monogastric animals. J Sci Food Agric. https://doi.org/10.1002/jsfa.9143
11. Ponthier E, Domínguez H, Torres MD (2020) The microwave assisted extraction sway on the features of antioxidant compounds and gelling biopolymers from *Mastocarpus stellatus*. Algal Res 51:102081. https://doi.org/10.1016/J.ALGAL.2020.102081
12. Chan PT, Matanjun P (2017) Chemical composition and physicochemical properties of tropical red seaweed, *Gracilaria changii*. Food Chem 221:302–310. https://doi.org/10.1016/j.foodchem.2016.10.066
13. Martínez-Sanz M, Gómez-Mascaraque LG, Ballester AR et al (2019) Production of unpurified agar-based extracts from red seaweed *Gelidium sesquipedale* by means of simplified extraction protocols. Algal Res 38:101420. https://doi.org/10.1016/j.algal.2019.101420
14. Ferreira LS, Silva TR, Santos JRD et al (2019) Structure, magnetic behavior and OER activity of CoFe2O4 powders obtained using agar-agar from red seaweed (Rhodophyta). Mater Chem Phys 237:121847. https://doi.org/10.1016/J.MATCHEMPHYS.2019.121847
15. Trigueros E, Sanz MT, Filipigh A et al (2021) Enzymatic hydrolysis of the industrial solid residue of red seaweed after agar extraction: extracts characterization and modelling. Food Bioprod Process 126:356–366. https://doi.org/10.1016/j.fbp.2021.01.014
16. da Rocha M, Alemán A, Romani VP et al (2018) Effects of agar films incorporated with fish protein hydrolysate or clove essential oil on flounder (*Paralichthys orbignyanus*) fillets shelf-life. Food Hydrocoll 81:351–363. https://doi.org/10.1016/J.FOODHYD.2018.03.017
17. Martínez-Sanz M, Martínez-Abad A, López-Rubio A (2019) Cost-efficient bio-based food packaging films from unpurified agar-based extracts. Food Packag Shelf Life 21:100367
18. Roy S, Rhim JW (2019) Agar-based antioxidant composite films incorporated with melanin nanoparticles. Food Hydrocoll 94:391–398. https://doi.org/10.1016/j.foodhyd.2019.03.038
19. Wang X, Guo C, Hao W et al (2018) Development and characterization of agar-based edible films reinforced with nano-bacterial cellulose. Int J Biol Macromol 118:722–730. https://doi.org/10.1016/j.ijbiomac.2018.06.089
20. Benito-González I, Jaén-Cano CM, López-Rubio A et al (2020) Valorisation of vine shoots for the development of cellulose-based biocomposite films with improved performance and bioactivity. Int J Biol Macromol 165:1540–1551. https://doi.org/10.1016/j.ijbiomac.2020.09.240
21. Kumar V, Fotedar R (2009) Agar extraction process for Gracilaria cliftonii (Withell, Millar, & Kraft, 1994). Carbohydr Polym 78:813–819. https://doi.org/10.1016/j.carbpol.2009.07.001
22. Quemener B, Lahaye M (1998) Comparative analysis of sulfated galactans from red algae by reductive hydrolysis and mild methanolysis coupled to two different HPLC techniques. J Appl Phycol 10(1):75–81

23. Stevenson TT, Furneaux RH (1991) Chemical methods for the analysis of sulphated galactans from red algae. Carbohydr Res 210:277–298. https://doi.org/10.1016/0008-6215(91)80129-B
24. AOAC (1990) AOAC: Official Methods of Analytical Chemist. Assoc Off Anal Chem
25. Singleton VL, Orthofer R, Lamuela-Raventós RM (1999) [14] Analysis of total phenols and other oxidation substrates and antioxidants by means of folin-ciocalteu reagent. Methods in enzymology. Elsevier, Amsterdam, pp 152–178
26. Re R, Pellegrini N, Proteggente A et al (1999) Antioxidant activity applying an improved ABTS radical cation decolorization assay. Free Radic Biol Med 26:1231–1237
27. Kieffer J, Wright JP (2013) PyFAI: A python library for high performance azimuthal integration on GPU. Powder Diffr. https://doi.org/10.1017/S0885715613000924
28. Ilavsky J, Jemian PR (2009) Irena: tool suite for modeling and analysis of small-angle scattering. J Appl Crystallogr 42:347–353
29. Álvarez-Viñas M, Flórez-Fernández N, Torres MD, Domínguez H (2019) Successful approaches for a red seaweed biorefinery. Mar Drugs 17:620. https://doi.org/10.3390/md17110620
30. Cavaco M, Duarte A, Freitas MV et al (2021) Seasonal nutritional profile of gelidium corneum (Rhodophyta, gelidiaceae) from the center of Portugal. Foods. https://doi.org/10.3390/FOODS10102394
31. Nunraksa N, Rattanasansri S, Praiboon J, Chirapart A (2019) Proximate composition and the production of fermentable sugars, levulinic acid, and HMF from Gracilaria fisheri and Gracilaria tenuistipitata cultivated in earthen ponds. J Appl Phycol 31:683–690. https://doi.org/10.1007/s10811-018-1552-9
32. Siddhanta AK, Prasad K, Meena R et al (2009) Profiling of cellulose content in Indian seaweed species. Bioresour Technol 100:6669–6673
33. Lozano I, Wacyk JM, Carrasco J, Cortez-San Martín MA (2016) Red macroalgae Pyropia columbina and Gracilaria chilensis: sustainable feed additive in the Salmo salar diet and the evaluation of potential antiviral activity against infectious salmon anemia virus. J Appl Phycol 28:1343–1351. https://doi.org/10.1007/s10811-015-0648-8
34. Banerjee K, Ghosh R, Homechaudhuri S, Mitra A (2009) Seasonal variation in the biochemical composition of red seaweed (Catenella repens) from Gangetic delta, northeast coast of India. J Earth Syst Sci 118:497–505. https://doi.org/10.1007/s12040-009-0045-2
35. Naseri A, Løvstad Holdt S, Jacobsen C (2019) Biochemical and nutritional composition of industrial red seaweed used in carrageenan production. J Aquat Food Prod Technol 28:967–973. https://doi.org/10.1080/10498850.2019.1664693
36. Chan PT, Matanjun P, Yasir SM, Tan TS (2015) Antioxidant activities and polyphenolics of various solvent extracts of red seaweed, *Gracilaria changii*. J Appl Phycol 27:2377–2386. https://doi.org/10.1007/s10811-014-0493-1
37. Ortiz-Viedma J, Aguilera JM, Flores M et al (2021) Protective effect of red algae (Rhodophyta) extracts on essential dietary components of heat-treated salmon. Antioxidants. https://doi.org/10.3390/antiox10071108
38. Sanz-Pintos N, Pérez-Jiménez J, Buschmann AH et al (2017) Macromolecular antioxidants and dietary fiber in edible seaweeds. J Food Sci 82:289–295. https://doi.org/10.1111/1750-3841.13592
39. de Oliveira JP, Bruni GP, Fabra MJ et al (2019) Development of food packaging bioactive aerogels through the valorization of *Gelidium sesquipedale* seaweed. Food Hydrocoll 89:337–350
40. Martínez-Sanz M, Ström A, Lopez-Sanchez P et al (2020) Advanced structural characterisation of agar-based hydrogels: Rheological and small angle scattering studies. Carbohydr Polym 236:115655. https://doi.org/10.1016/J.CARBPOL.2019.115655
41. Martínez-Sanz M, Mikkelsen D, Flanagan BM et al (2017) Multiscale characterisation of deuterated cellulose composite hydrogels reveals evidence for different interaction mechanisms with arabinoxylan, mixed-linkage glucan and xyloglucan. Polymer (Guildf) 124:1–11. https://doi.org/10.1016/J.POLYMER.2017.07.036
42. Duman O, Polat TG, Diker CÖ, Tunç S (2020) Agar/κ-carrageenan composite hydrogel adsorbent for the removal of Methylene Blue from water. Int J Biol Macromol 160:823–835. https://doi.org/10.1016/J.IJBIOMAC.2020.05.191
43. Shankar S, Teng X, Rhim JW (2014) Properties and characterization of agar/CuNP bionanocomposite films prepared with different copper salts and reducing agents. Carbohydr Polym 114:484–492. https://doi.org/10.1016/J.CARBPOL.2014.08.036
44. Raphael E, Avellaneda CO, Manzolli B, Pawlicka A (2010) Agar-based films for application as polymer electrolytes. Electrochim Acta 55:1455–1459. https://doi.org/10.1016/J.ELECTACTA.2009.06.010
45. Shankar S, Rhim JW (2016) Preparation of nanocellulose from micro-crystalline cellulose: the effect on the performance and properties of agar-based composite films. Carbohydr Polym 135:18–26. https://doi.org/10.1016/J.CARBPOL.2015.08.082
46. Guerrero P, Etxabide A, Leceta I et al (2014) Extraction of agar from *Gelidium sesquipedale* (Rodhopyta) and surface characterization of agar based films. Carbohydr Polym 99:491–498. https://doi.org/10.1016/j.carbpol.2013.08.049
47. Chen YW, Lee HV, Juan JC, Phang SM (2016) Production of new cellulose nanomaterial from red algae marine biomass Gelidium elegans. Carbohydr Polym 151:1210–1219. https://doi.org/10.1016/j.carbpol.2016.06.083
48. Chen B-K, Shen C-H, Chen S-C, Chen AF (2010) Ductile PLA modified with methacryloyloxyalkyl isocyanate improves mechanical properties. Polymer (Guildf) 51:4667–4672
49. Mathew AP, Oksman K, Sain M (2005) Mechanical properties of biodegradable composites from poly lactic acid (PLA) and microcrystalline cellulose (MCC). J Appl Polym Sci 97:2014–2025
50. Cyras VP, Manfredi LB, Ton-That M-T, Vázquez A (2008) Physical and mechanical properties of thermoplastic starch/montmorillonite nanocomposite films. Carbohydr Polym 73:55–63
51. Majdzadeh-Ardakani K, Navarchian AH, Sadeghi F (2010) Optimization of mechanical properties of thermoplastic starch/clay nanocomposites. Carbohydr Polym 79:547–554
52. Makwana D, Castaño J, Somani RS, Bajaj HC (2020) Characterization of Agar-CMC/Ag-MMT nanocomposite and evaluation of antibacterial and mechanical properties for packaging applications. Arab J Chem 13:3092–3099. https://doi.org/10.1016/J.ARABJC.2018.08.017
53. Rhim JW (2011) Effect of clay contents on mechanical and water vapor barrier properties of agar-based nanocomposite films. Carbohydr Polym 86:691–699. https://doi.org/10.1016/j.carbpol.2011.05.010
54. Martínez-Sanz M, Erboz E, Fontes C, López-Rubio A (2018) Valorization of Arundo donax for the production of high performance lignocellulosic films. Carbohydr Polym 199:276–285
55. Benito-González I, Martínez-Sanz M, Lopez-Rubio A (2018) Potential of lignocellulosic fractions from Posidonia oceanica to improve barrier and mechanical properties of bio-based packaging materials. Int J Biol Macromol 118:542–551. https://doi.org/10.1016/j.ijbiomac.2018.06.052
56. Guerrero P, Garrido T, Leceta I, De La Caba K (2013) Films based on proteins and polysaccharides: Preparation and physical-chemical characterization. Eur Polym J 49:3713–3721. https://doi.org/10.1016/j.eurpolymj.2013.08.014
57. Martínez-Sanz M, Lopez-Rubio A, Lagaron JM (2013) High-barrier coated bacterial cellulose nanowhiskers films with reduced moisture sensitivity. Carbohydr Polym 98:1072–1082. https://doi.org/10.1016/J.CARBPOL.2013.07.020